Korean J. Chem. Eng., 34(12), 3214-3219 (2017)
DOI: 10.1007/s11814-017-0225-8

pISSN: 0256-1115
eISSN: 1975-7220

Expanding depletion region via doping: Zn-doped Cu_2O buffer layer in Cu_2O photocathodes for photoelectrochemical water splitting

Kangha Lee*, Cheol-Ho Lee*,*, Jun Young Cheong**, Seokwon Lee*, Il-Doo Kim**, Han-Ik Joh***,****, and Doh Chang Lee*,†**

*Department of Chemical and Biomolecular Engineering (BK21+ Program), KAIST Institute for the Nanocentury, Korea Advanced Institute of Science and Technology (KAIST), Daejeon 34141, Korea
**Department of Materials Science and Engineering, Korea Advanced Institute of Science and Technology (KAIST), Daejeon 34141, Korea
***Carbon Convergence Materials Research Center, Institute of Advanced Composite Materials, Korea Institute of Science and Technology (KIST), Wanju, Jeollabukdo 55324, Korea
****Department of Extreme Energy Engineering, Konkuk University, Seoul 27478, Korea
(*Received 4 July 2017 • accepted 9 August 2017*)

Abstract−We report photoelectrochemical hydrogen evolution reaction using a Cu_2O-based photocathode with a layer doped with Zn ions. The doping results in the shift of the onset flat-band potential of the photocathode, likely a consequence of maximized band-bending in the Cu_2O/Zn : Cu_2O heterojunction. Systematic electrochemical analysis reveals that expansion of depletion region is responsible for the enhanced photoelectrochemical performance, e.g., the increase of photocurrent and reduced internal resistance.

Keywords: Cu_2O, Zn-doped Cu_2O, Photocathode, Water Splitting, Photoelectrochemistry

INTRODUCTION

Photoelectrochemical (PEC) conversion of water into hydrogen and oxygen molecules has received a tremendous amount of attention, deservingly so as the process utilizes abundant solar irradiation and the hydrogen molecules produced from the reaction can be used in a wide variety of petrochemical processes [1-4]. The awareness on hydrogen economy is ever-increasing by virtue of increasing volume of production for hydrocarbons, and consequently expanding demand on key reactant, hydrogen. Water splitting using a PEC reaction has also gained a great deal of interest, because of the pressing need to diversify the sources of hydrogen production, particularly the processes involving less CO_2-production concern. This interest leaves considerable research efforts in the development of photocathodes.

Among p-type semiconductors, cuprous oxide (Cu_2O) has been intensively studied, due to its low toxicity, high abundance and low processing cost [5-9]. However, the theoretical maximum photovoltage of Cu_2O in PEC water splitting is estimated to be *ca.* 0.6 V considering the difference between the Fermi level of p-type Cu_2O (−5.19 V) [10,11] and the hydrogen evolution potential (−4.50 eV at pH 0) [12]. The small photovoltage is bound to cause low solar-to-hydrogen (STH) conversion efficiency in the absence of external bias [13]. One solution to address this issue is to deposit a thin n-type buffer layer so as to make the valence and conduction bands sufficiently more negative than those of Cu_2O and form p-n junction to maximize the band bending within Cu_2O and achieve high STH efficiency. Bosco et al. introduced a thin ZnS layer on Cu_2O. ZnS has a valence band maximum of −7.58 eV and a conduction band minimum of −3.90 eV [14]. Dai et al. deposited ZnS layer (~5 nm) on Cu_2O by thermal evaporation deposition. With the ZnS buffer layer, the photovoltage of photocathode increased to 0.71 V from 0.59 V [15]. Li et al. deposited Ga_2O_3 layer on Cu_2O nanowires via atomic layer deposition (ALD), and onset voltage shifted markedly to 1.02 V vs. RHE and the photocathode with Ga_2O_3 produced a photocurrent of −2.95 mA cm^{-2} at 0 V vs. RHE with a conversion efficiency of 0.78% at 0.45 V vs. RHE [13,16]. But ZnS or Ga_2O_3 crystals, as efficient as they are in terms of band bending, are expected to cause lattice strain at their interface with Cu_2O [17,18]. This explains why the previous reports on these heterostructures have been limited to thin layer of these n-type crystals, while increasing the length of depletion region would be necessary to maximize the band-bending. A key strategy to minimize the lattice strain is to use Cu_2O crystal with impurity atoms doped within.

There have been reports on Cu_2O doped with various group IV elements such as Co [19], In [20], Al [19], Mn [21], and Zn [19,22-26]. Notably, Zn-doped Cu_2O (Zn : Cu_2O) demonstrates improved performance in photovoltaics [26], photocatalytic and PEC hydrogen generation [22,25]. Zhang et al. synthesized Zn-doped Cu_2O microcubes and reported remarkable enhancement of photocatalytic activity of Cu_2O. Cu_2O with 0.1 wt% of Zn dopant showed an apparent quantum yield of 38.95% [25]. Hu et al., who further applied Zn : Cu_2O to PEC system, developed a facile Zn-doping electrodeposition approach to improve the photostability of Cu_2O photocathodes in PEC water splitting [22]. In addition, Zhu et al. in-

†To whom correspondence should be addressed.
E-mail: dclee@kaist.edu
‡The authors declare no competing financial interest.

troduced Zn : Cu_2O layer to photovoltaics, in which higher Fermi level positioning and improved conductivity in the Zn : Cu_2O films enabled substantially improved performance in an electrodeposited Cu_2O homojunction photovoltaic device [26].

Herein, we introduce thin Zn : Cu_2O buffer layer on Cu_2O photocathode for PEC water splitting to maximize band bending within Cu_2O resulting in enhancement of photovoltage and charge separation. To elucidate the role of Zn : Cu_2O buffer layer, various electrochemical analyses are presented, particularly in the context of depletion region.

EXPERIMENTAL SECTION

1. Materials

The following chemicals were purchased from Sigma-Aldrich and used without additional treatment: copper(II) sulfate pentahydrate ($CuSO_4 \cdot 5H_2O$, ≥99.99%), sodium hydroxide (NaOH, ≥97%), sodium DL-lactate (60 wt% in H_2O), sodium acetate (CH_3COONa, ≥99.9%), sodium perchlorate ($NaClO_4$, ≥98.0%), zinc nitrate hexahydrate ($Zn(NO_3)_2 \cdot 6H_2O$, ≥98%), potassium bicarbonate ($KHCO_3$, 99.7%), sodium sulfate (Na_2SO_4, ≥99.9%), potassium phosphate monobasic (KH_2PO_4, ≥99.9%), ammonium tetrathiomlybdate ($(NH_4)_2MoS_4$, ≥99.97%) and tetrakis(dimethylamido)titanium (IV) (TDMAT, 99.999%). Ammonium hydroxide (NH_4OH, 25-28%) was purchased from Daejung. Multiwall carbon nanotube (MWCNT, TMC 220-05) was purchased from Nano Solution.

2. Electrodeposition of Cu_2O and Zn : Cu_2O

Both Cu_2O and Zn : Cu_2O layers were electrodeposited by using a conventional three-electrode cell with a platinum coil counter electrode and a Ag/AgCl (3 M NaCl solution) reference electrode at 60 °C. The electrodeposition solution for Cu_2O layer contained: 0.02 M copper (II) sulface pentahydrate, and 0.34 M sodium lactate; the pH was adjusted to 11 using dilute NaOH. The FTO working electrode potential was held at −0.4 V vs. Ag/AgCl. Electrodeposition solutions for the Zn : Cu_2O layers contained: 0.01 M copper sulfate pentahydrate, 0.1 M sodium acetate, 0.03 M zinc nitrate, and 0.004 M sodium perchlorate. Zn : Cu_2O film was deposited using an applied potential of −0.1 V vs. Ag/AgCl at pH 5.80.

3. Atomic Layer Deposition of TiO_2

TiO_2 was coated on photocathodes with active materials by using atomic layer deposition (ALD). ALD process was carried out in the ALD system (DAEKI HI-TECH, Co., Ltd., Korea) at temperatures at 80 °C (TDMAT) was used as the Ti precursor and the reaction chamber was maintained at 10^{-3} Torr with steady N_2/H_2 plasma reactant gas. The TiO_2 coating layer was made by simultaneously changing H_2O and N_2/H_2 reactant gas. The number of ALD cycles was in the range between 50 to 100 cycles.

4. Synthesis of O-CNT/Mo_3S_{13} Catalyst

Synthesis of Mo_3S_{13}: 0.1 g of MoS_3 was dispersed in 40 ml of 25-28% ammonium hydroxide solution by bath-sonication for 10 min. Then, the mixture was kept for seven days at room temperature. Finally, precipitates were collected by filtration and washed using DI water followed by freeze-drying.

Oxidation of MWCNT: 0.1 g of MWCNT was dispersed in 100 ml of HNO_3 (30 wt%) and H_2SO_4 (70 wt%) mixture by batch sonication. The mixture was refluxed under magnetic stirring for 6 h at 50 °C. The resulting suspension was then diluted by adding DI water slowly. Finally, O-CNT was obtained by filtration and washed using DI water followed by drying in vacuum oven at 60 °C.

5. Physiochemical Characterization

Different types of photocathodes were characterized by X-ray photoelectron spectroscopy (XPS), and X-ray diffraction (XRD). XPS measurements were performed with a Sigma Probe (Thermo VG Scientific). XRD measurements were performed with an Ultima IV (RIGAKU) operated with a CuKα source (λ=1.54 Å). The data were collected with a scan rate of 3° min^{-1} ranging from 20 to 70°.

6. PEC Measurements

PEC reaction was conducted in a three-electrode configuration cell using a Pt coil as the counter electrode and Ag/AgCl (3 M NaCl) as the reference electrode. The potential measured using a Ag/AgCl reference electrode was converted to the reversible hydrogen electrode (RHE) using the following formula:

$$E_{RHE}=E_{Ag/AgCl}+0.197+0.059pH$$

Different photocathodes with an exposed surface area of 1 cm^2 were connected to custom-made Pyrex reactor. An aqueous solution of 0.5 M Na_2SO_4 and 0.1 M KH_2PO_4 (pH 4.25) was used as the electrolyte during the measurement. Linear sweep voltammetry (LSV) was carried out using a VERTEX potentiostat (Ivium Technologies) at a scan rate of 20 mV s^{-1} under a chopped illumination of 100 mW cm^{-2} (using LS 150 with AM1.5G filter, Abet Technologies).

7. Impedance Measurements

The electrochemical impedance measurements involved using the same experimental setup. The Nyquist plots were obtained in the dark and under AM1.5G illumination at an applied potential of 0, 0.3 and 0.6 V (vs. RHE) within the frequency range of 1 MHz to 1 Hz using an amplitude of 10 mV. The Mott-Schottky analysis was run with the potential range of 0.4 to 0.7 V (vs. RHE) was performed at 1 kHz.

RESULTS AND DISCUSSION

To maximize the band bending of p-type Cu_2O without significant lattice mismatch, we introduced thin Zn : Cu_2O buffer layer on electro-deposited Cu_2O film. At the same time, to address the issue of stability in Cu_2O-based photocathodes, atomic layer deposition (ALD) of TiO_2 was employed [27,28]. O-CNT/Mo_3S_{13} catalyst was also adopted to promote the hydrogen evolution reaction (HER) at photocathode/electrolyte interface. First, we investigated whether the introduction of Zn : Cu_2O buffer layer indeed induces the band bending within Cu_2O. The key in PEC buffer layer is to deposit the top layer as uniform as possible since the primary role of buffer layer is to increase band bending within a thicker Cu_2O. In addition, the buffer layer should be thin enough, since the electron transfer at semiconductor/electrolyte interface could be impeded due to the formation of a Schottky barrier in the thick buffer layer (Fig. S1 in the Supporting information) [15]. As shown in Fig. 1, without Zn : Cu_2O buffer layer, pure Cu_2O photocathode exhibits cathodic photo-response around 0.7 V vs. RHE, and maximum photocurrent density of *ca.* 2 mA cm^{-2} at 0 V vs. RHE. In addition, ranging from 0.7 to 0 V, the photocurrent increases mono-

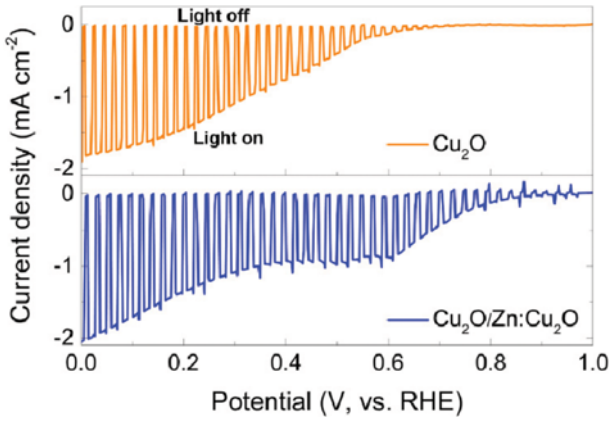

Fig. 1. Light chopped linear sweep voltammetry curve of Cu_2O (orange) and Zn : Cu_2O/Cu_2O (blue) in 0.5 M Na_2SO_4 and 0.1 M KH_2PO_4 solution.

tonically, which means the fill factor of photocathode is relatively low. On the contrary, Zn : Cu_2O ad-layer enhances both onset potential and photocurrent density. Notably, the onset potential can be extended to *ca.* 1 V vs. RHE with the significant increase of the photocurrent density over the positive potential range (0.6-1 V vs. RHE). For instance, at 0.6 V, vs. RHE, the photocurrent of Zn : Cu_2O/Cu_2O is 0.88 mA cm^{-2}, which is over seven-times higher than the one of pure Cu_2O. We believe that this is due to the increased band bending within Cu_2O layer with proper thickness of buffer layer.

It has been reported that this early onset and increased photo-

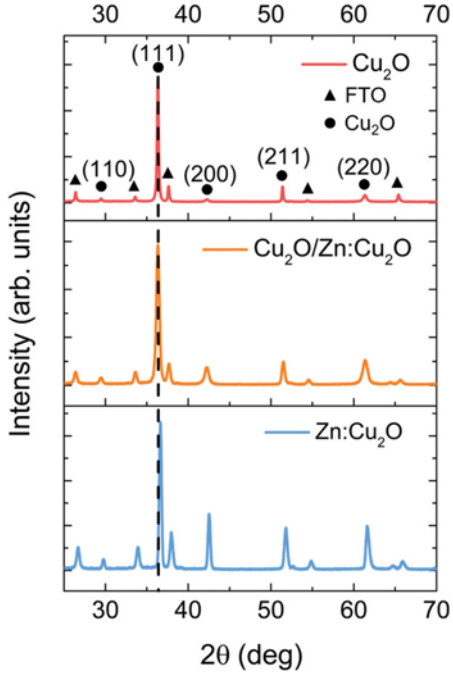

Fig. 2. X-ray diffraction patterns of Cu_2O (red), Cu_2O/Zn : Cu_2O (orange), and Zn : Cu_2O (sky blue) deposited on FTO glass.

activity extending over the positive potential range (0.6-1 V vs. RHE) can be achieved by reducing the conduction band misfit and defective interface, through the introduction of Ga_2O_3 buffer layer

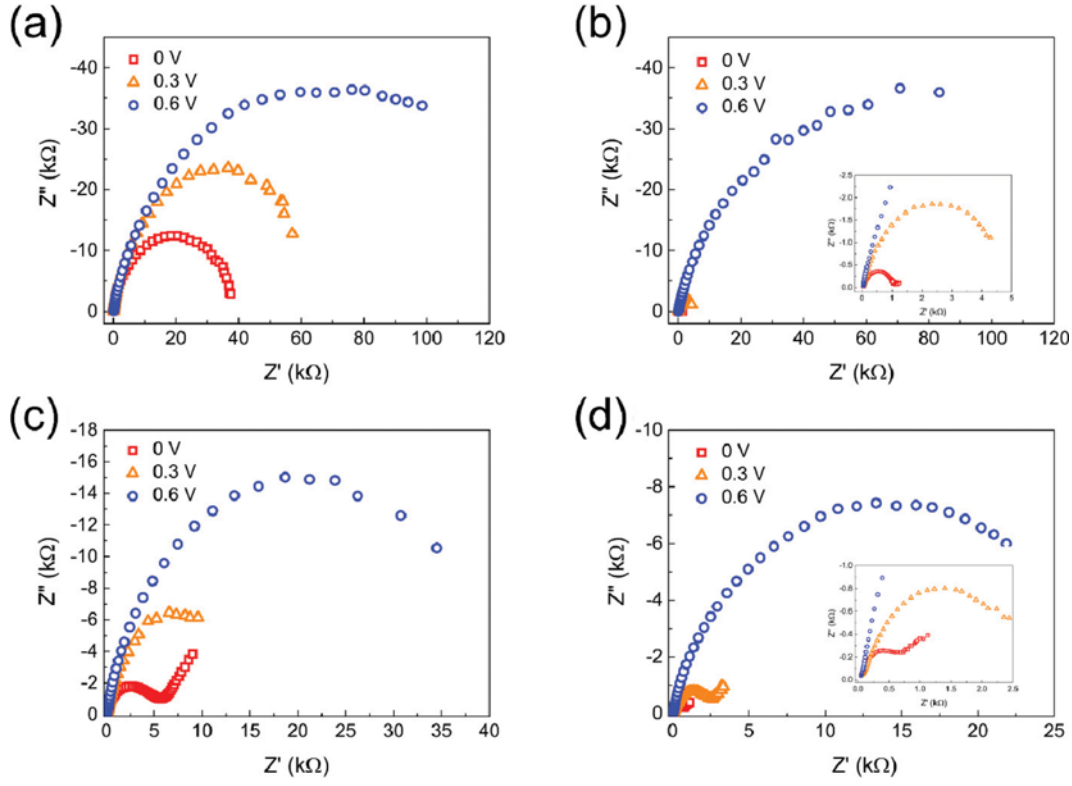

Fig. 3. Nyquist plot of Cu_2O (a) in the dark and (b) under AM 1.5G irradiation, and Zn : Cu_2O (c) in the dark and (d) under AM 1.5G irradiation at 0, 0.3, and 0.6 V vs. RHE.

Table 1. Summary of charge transfer resistance at 0, 0.3, and 0.6 V vs. RHE (unit: kΩ cm^{-2})

Potential (V, vs. RHE)	Cu_2O		$Zn:Cu_2O/Cu_2O$	
	Dark	Irradiation	Dark	Irradiation
0	22.106	0.568	3.279	0.420
0.3	35.438	2.511	7.630	1.445
0.6	75.241	74.971	21.480	17.114

[13]. Considering the homo-junction nature of our buffer layer system, the conduction band misfit can be excluded. Thus, we investigated the lattice misfit between Cu_2O and $Zn:Cu_2O$.

XRD analysis reveals that all peaks are assigned to cubic Cu_2O or FTO substrate, and there is no peak assigned to pure ZnO (Fig. 2). This suggests that Zn ions are incorporated into the Cu_2O lattice [29], which is well matched with XPS analysis (Fig. S2 in the Supporting Information). In addition, bare Cu_2O and $Zn:Cu_2O$ show only 0.3° of (111) peak shift, which corresponds to 0.04 Å of lattice change. Indeed, it is reasonable that ionic radius of Cu^+ and Zn^{2+} cations are 0.46 and 0.4 Å, respectively, which is similar in size [23].

To gain more insight into the effect of $Zn:Cu_2O$ buffer layer on the carrier kinetics, we used impedance spectroscopy to measure the charge transfer resistance (R_{ct}) of photocathode. Fig. 3 shows the Nyquist plot of Cu_2O and $Zn:Cu_2O$ photocathodes in the dark and under AM 1.5G irradiation at various potentials; the results are summarized in Table 1. In the Nyquist plot, the high-frequency limit shows the overall ohmic resistance (R_s) including semiconductor, wire connection, and electrolyte. On the other hand, the semi-circular feature in low frequency region describes charge transfer at the semiconductor/electrolyte interface with RC parallel circuit, where R is the charge transfer resistance and C is the capacitance [30]. After adopting $Zn:Cu_2O$ layer, R_{ct} at various potentials decrease in the dark. For example, R_{ct} of Cu_2O are 22.106 and 75.241 kΩ cm^{-2} at 0 and 0.6 V, whereas ones of $Cu_2O/Zn:Cu_2O$ are 3.279 and 21.480 kΩ cm^{-2} at 0 and 0.6 V, respectively. The reduction of R_{ct} over the entire potential range implies that the charge carriers within photocathode are more efficiently separated and transferred due to the band-bending through $Zn:Cu_2O$ buffer layer.

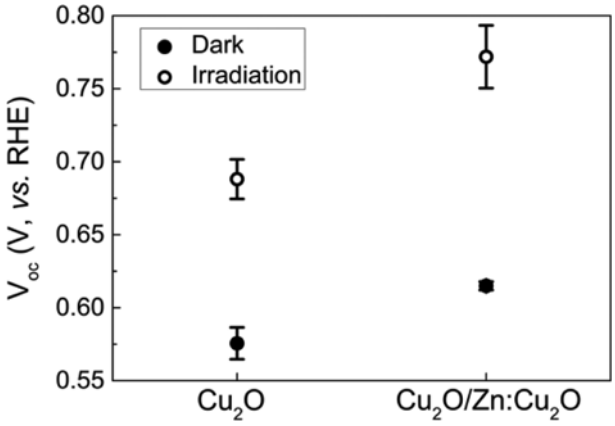

Fig. 4. Average open-circuit potential of Cu_2O and $Zn:Cu_2O$ photocathodes in the dark and under AM 1.5G irradiation. V_{oc} of five different photocathode was measured and averaged.

Remarkably, this enhancement becomes more obvious under irradiation at the low bias region. Specifically, R_{ct} at 0 and 0.3 V vs. RHE from both types of films are dramatically reduced due to the photo-generation of charge carriers. In stark contrast, there is almost no change at 0.6 V vs RHE where there is no photo-response, while with $Zn:Cu_2O$ buffer layer, the resistance is reduced by 20%. Therefore, it can be concluded that $Zn:Cu_2O$ layer facilitates the charge separation and transfer, which is extended to the lower-bias region.

To further verify how the $Zn:Cu_2O$ buffer layer pushes the operation condition toward the lower bias, we quantified the open-circuit potential (V_{oc}) in the dark and under irradiation. V_{oc} was monitored by measuring the potentials at zero net current densities, where the kinetic factor does not have a critical role [15,31]. To acquire more reliable results, we measured V_{oc} of five different photocathodes for Cu_2O and $Zn:Cu_2O$, respectively. As shown in Fig. 4, V_{oc} with $Zn:Cu_2O$ shift to 0.61 V from 0.58 V in the dark. The shift of V_{oc} in the dark can be explained by the shift of flat band potential (V_{fb}) after $Zn:Cu_2O$ deposition. V_{oc} in the dark is defined as the difference between V_{fb} and the redox potential of the HER. Since the theoretical reduction potential of HER is 0 V vs. RHE, we can consider V_{oc} under dark is the same as V_{fb}, and the values are well matched with the measured V_{fb} (Fig. 5(a)). Under illumina-

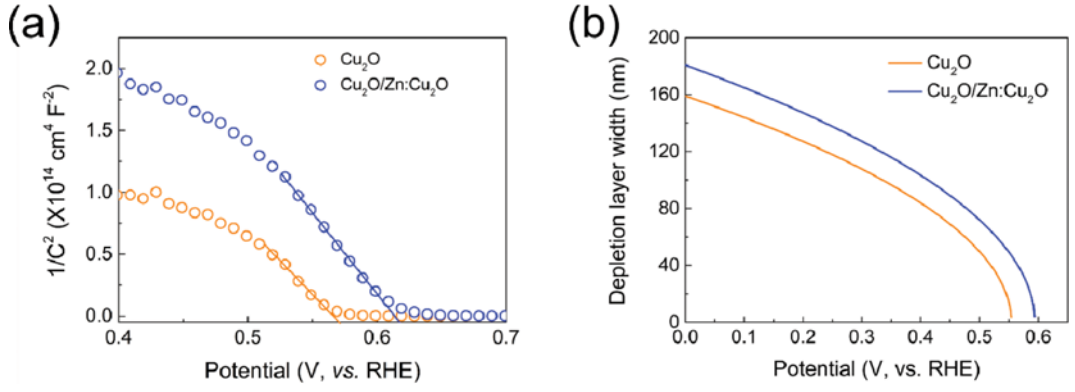

Fig. 5. (a) Mott-Schottky plots of Cu_2O and $Zn:Cu_2O$ photocathodes without TiO_2 protective layer, and (b) calculated depletion layer width based on Mott-Schottky analysis.

tion, photo-generated electrons in the conduction band and depletion layer split the quasi-Fermi levels of charge carriers. This split causes the flattening of the band and the measured V_{oc} means the Fermi level of holes in Cu_2O [15]. Under irradiation, it is expected that the Fermi level of Cu_2O shifts toward the positive direction. The measured V_{oc} in Fig. 4 indeed moves in the positive direction and the values are 0.69 and 0.77 V vs. RHE for Cu_2O and Zn : Cu_2O, respectively. The difference of V_{oc} in the dark and under irradiation demonstrates the photovoltage generated by the semiconductor/electrolyte interface. The measured photovoltages of Cu_2O and Cu_2O/Zn : Cu_2O photocathodes are 112.5±18.2 and 157.8±21.5 mV, respectively. After introduction of buffer layer, photovoltage increases by 45.3 mV. The value of photovoltage presents the position of conduction band energy level and the degree of band bending. Therefore, increased photovoltage by Zn : Cu_2O also supports that the buffer layer maximizes the degree of band bending within Cu_2O.

Finally, to quantify the degree of band bending within Cu_2O, we performed Mott-Schottky analysis and calculated the depletion layer width (W_D). For a p-type semiconductor, the electric field is induced in the semiconductor near semiconductor/electrolyte interface caused by the charge depletion. This depletion is the origin of the band bending. Specifically, the photo-generated electrons in the depletion region or the electrons diffuse from bulk to depletion layer are assumed to generate the photocurrent. Considering the short diffusion length of minority carrier (electron) of Cu_2O ranging from 10 to 100 nm [32], the W_D can play a critical role in the collection of charge carriers. To calculate the W_D of Cu_2O before and after Zn : Cu_2O deposition, we did Mott-Schottky analysis without TiO_2 protective layer. Since n-type depletion layer by amorphous ALD TiO_2 is very short (~2 nm) when the electron quasi-Fermi level is at 0 V, vs. RHE, we can assume that Cu_2O based semiconductor layer directly forms Fermi level equilibrium with the reduction potential of HER and TiO_2 does not affect the formation of depletion layer within Cu_2O [16].

The Mott-Schottky plot in Fig. 5(a) was analyzed using the modified Mott-Schottky equation: [33]

$$1/C_{sc}^2=(2/e\varepsilon\varepsilon_0N_A)(V-V_{fb}-kT/e) \quad (1)$$

where C_{sc} are the space-charge capacitance (in F/cm^2); e is the electronic charge (in C); ε is the relative dielectric constant of semiconductors; ε_0 is the permittivity of vacuum; N_A is the carrier density (in cm^{-3}); E_{fb} is the flat-band potential (in V); k is the Boltzmann constant; and T is temperature (in K). ε for Cu_2O was selected to be 7.5 [34], and the V_{fb} is obtained from the intercept of the linear part of curves with x-axis. The measured V_{fb} for Cu_2O and Zn : Cu_2O are 0.58 and 0.62 V vs. RHE with 1.82×10^{16} and 1.51×10^{16} cm^{-3} of carrier concentration, respectively. The shift of V_{fb} to positive potential with Zn : Cu_2O buffer layer indicates that Zn : Cu_2O/Cu_2O photocathode has larger built-in potential than bare Cu_2O photocathode. This behavior is similar to that of p-n homojunction between p-Cu_2O and n-Cu_2O [35]. The lower concentration of carrier (hole) may be due to the fewer defect sites in Zn : Cu_2O/Cu_2O per unit volume [36]. In general, it is accepted that p-type behavior of Cu_2O originates from the vacancies on the Cu sites in the crystal [37]. With Zn dopant, the possibility that the Cu vacancies are substituted by Zn^{2+} cation becomes high since the binding energy between Zn and O (530.5 eV) is smaller than that between Cu and O (943.0 eV) and ionic radius of Zn^{2+} is also smaller than that of Cu^+ [23,38,39]. Therefore, the reduced carrier density is due to the lower concentration of Cu vacancy sites with Zn : Cu_2O layer.

Based on the results of Mott-Schottky analysis, we calculated the W_D using following equation:

$$W_D=\left[\frac{2\varepsilon_0\varepsilon}{eN_A}\left(-V+V_{fb}+\frac{kT}{e}\right)\right]^{1/2} \quad (2)$$

The calculation results are shown in Fig. 5(b). The difference of W_D between Cu_2O and Zn : Cu_2O at 0 V vs. RHE is 22 nm, and the value reaches 46 nm at V_{fb} of Cu_2O. Considering the relatively short electron diffusion length in Cu_2O, the difference can be influential. In a PEC water splitting system, photocurrent density and quantum efficiency are determined by the depletion layer. As in Gärtner's model [40], photocurrent density (J) can be expressed by $J=J_{DL}+J_{DIFF}$, where J_{DL} is the drift current density due to carrier generated in the depletion regime and J_{DIFF} is the diffusion current density of electron generated outside the depletion layer [41]. Since the diffusion length of electrons in Cu_2O is very short (10 to 100 nm) [32], J_{DL} is a major factor that determines the photocurrent density and can be expressed by following equation:

$$J_{DL}=e\int_0^{W_D}G(x)dx, \quad (3)$$

where G(x) is the generation rate of electrons, and is at the semiconductor/electrolyte interface. Because the thickness of Cu_2O is too thick compared with that of Zn : Cu_2O, we can assume that the electron generation by Zn : Cu_2O layer is negligible (Fig. S3 in the Supporting information), so we can consider that G(x) is the same in both photocathodes. Therefore, J_{DL} is the only function of W_D. In addition, the quantum efficiency (η) of PEC system can be expressed in terms of W_D: [42]

$$\eta=W_DA_n\frac{(h\nu-E_g)^n}{h\nu}, \quad (4)$$

where $h\nu$ is the photon energy, n is the transition order number, E_g is the band gap of the semiconductor, and A_n is a constant. In this equation, the only variable is W_D since E_g of light harvesting layer is the same in both photocathodes, as discussed above. Therefore, W_D is the most important factor to determine the performance of photocathode. Typically, in more positive potential range than 0.3 V, where the effect of Zn : Cu_2O stands out, *ca.* 20 nm of W_D difference can be critical because W_D of Cu_2O is shorter than 100 nm. Therefore, we can conclude that effect of Zn : Cu_2O buffer layer is mainly from the maximized band bending within Cu_2O by the increased W_D.

CONCLUSION

We have successfully introduced Zn : Cu_2O thin buffer layer via electrodeposition method for maximizing band bending within Cu_2O photocathode. With Zn : Cu_2O buffer layer, the photocathode showed photo-response from ca. 1 V vs. RHE and the V_{fb} was shifted to 0.62 V from 0.58 V. In addition, the generated photovolt-

age of Zn : Cu_2O/Cu_2O photocathode increased to 157.8 mV, whereas that of Cu_2O was 112.5 mV. In impedance analysis, charge transfer kinetics is also with Zn : Cu_2O buffer layer enhanced over the entire potential range both in the dark and under illumination. All these effects of Zn : Cu_2O buffer layer are attributed to the increased degree of band bending within Cu_2O originated from expanded depletion layer. Based on our results, it is expected that we can run PEC water splitting reaction and get improved STH efficiency without external bias by combining the Zn : Cu_2O/Cu_2O photocathode and a previously developed photoanode.

ACKNOWLEDGEMENT

This work was supported by the National Research Foundation (NRF) grants funded by the Korean government (no. NRF-2017R1A2B2011066).

SUPPORTING INFORMATION

Additional information as noted in the text. This information is available via the Internet at http://www.springer.com/chemistry/journal/11814.

REFERENCES

1. N. S. Lewis and D. G. Nocera, *Proc. Natl. Acad. Sci.*, **103**, 15729 (2006).
2. M. Graetzel, *Acc. Chem. Res.*, **14**, 376 (1981).
3. O. Khaselev and J. A. Turner, *Science*, **280**, 425 (1998).
4. M. G. Walter, E. L. Warren, J. R. McKone, S. W. Boettcher, Q. Mi, E. A. Santori and N. S. Lewis, *Chem. Rev.*, **110**, 6446 (2010).
5. J. Luo, L. Steier, M.-K. Son, M. Schreier, M. T. Mayer and M. Grätzel, *Nano Lett.*, **16**, 1848 (2016).
6. A. Paracchino, N. Mathews, T. Hisatomi, M. Stefik, S. D. Tilley and M. Grätzel, *Energy Environ. Sci.*, **5**, 8673 (2012).
7. M. Schreier, P. Gao, M. T. Mayer, J. Luo, T. Moehl, M. K. Nazeeruddin, S. D. Tilley and M. Grätzel, *Energy Environ. Sci.*, **8**, 855 (2015).
8. A. A. Dubale, W.-N. Su, A. G. Tamirat, C.-J. Pan, B. A. Aragaw, H.-M. Chen, C.-H. Chen and B.-J. Hwang, *J. Mater. Chem. A*, **2**, 18383 (2014).
9. K. Lee, S. Lee, H. Cho, S. Jeong, W. D. Kim, S. Lee and D. C. Lee, *J. Energy Chem.* (2017), DOI:10.1016/j.jechem.2017.04.019.
10. L. I. Bendavid and E. A. Carter, *J. Phys. Chem. B*, **117**, 15750 (2013).
11. A. Paracchino, V. Laporte, K. Sivula, M. Grätzel and E. Thimsen, *Nature Mater.*, **10**, 456 (2011).
12. S. D. Tilley, M. Schreier, J. Azevedo, M. Stefik and M. Graetzel, *Adv. Funct. Mater.*, **24**, 303 (2014).
13. C. Li, T. Hisatomi, O. Watanabe, M. Nakabayashi, N. Shibata, K. Domen and J.-J. Delaunay, *Energy Environ. Sci.*, **8**, 1493 (2015).
14. J. P. Bosco, S. B. Demers, G. M. Kimball, N. S. Lewis and H. A. Atwater, *J. Appl. Phys.*, **112**, 093703 (2012).
15. P. Dai, W. Li, J. Xie, Y. He, J. Thorne, G. McMahon, J. Zhan and D. Wang, *Angew. Chem. Int. Ed.*, **53**, 13493 (2014).
16. C. Li, T. Hisatomi, O. Watanabe, M. Nakabayashi, N. Shibata, K. Domen and J.-J. Delaunay, *Appl. Phys. Lett.*, **109**, 033902 (2016).
17. D. Aspnes, *Surf. Sci.*, **132**, 406 (1983).
18. S. Hussain, C. Cao, Z. Usman, Z. Chen, G. Nabi, W. S. Khan, Z. Ali, F. K. Butt and T. Mahmood, *Thin Solid Films*, **522**, 430 (2012).
19. S. N. Kale, S. B. Ogale, S. R. Shinde, M. Sahasrabuddhe, V. N. Kulkarni, R. L. Greene and T. Venkatesan, *Appl. Phys. Lett.*, **82**, 2100 (2003).
20. X.-M. Cai, X.-Q. Su, F. Ye, H. Wang, X.-Q. Tian, D.-P. Zhang, P. Fan, J.-T. Luo, Z.-H. Zheng, G.-X. Liang and V. A. L. Roy, *Appl. Phys. Lett.*, **107**, 083901 (2015).
21. M. Wei, N. Braddon, D. Zhi, P. A. Midgley, S. K. Chen, M. G. Blamire and J. L. MacManus-Driscoll, *Appl. Phys. Lett.*, **86**, 072514 (2005).
22. F. Hu, Y. Zou, L. Wang, Y. Wen and Y. Xiong, *Int. J. Hydrogen Energy*, **41**, 15172 (2016).
23. A. Ravichandran, K. Dhanabalan, K. Ravichandran, R. Mohan, K. Karthika, A. Vasuhi and B. Muralidharan, *Acta Metal. Sin. (Engl. Lett.)*, **28**, 1041 (2015).
24. F. Ye, X.-Q. Su, X.-M. Cai, Z.-H. Zheng, G.-X. Liang, D.-P. Zhang, J.-T. Luo and P. Fan, *Thin Solid Films*, **603**, 395 (2016).
25. L. Zhang, D. Jing, L. Guo and X. Yao, *ACS Sustainable Chem. Eng.*, **2**, 1446 (2014).
26. C. Zhu and M. J. Panzer, *ACS Appl. Mater. Interfaces*, **7**, 5624 (2015).
27. A. Paracchino, V. Laporte, K. Sivula, M. Grätzel and E. Thimsen, *Nature Mater.*, **10**, 456 (2011).
28. A. Paracchino, N. Mathews, T. Hisatomi, M. Stefik, S. D. Tilley and M. Gratzel, *Energy Environ. Sci.*, **5**, 8673 (2012).
29. B. Heng, T. Xiao, W. Tao, X. Hu, X. Chen, B. Wang, D. Sun and Y. Tang, *Crystal Growth Design*, **12**, 3998 (2012).
30. L. Bertoluzzi and J. Bisquert, *J. Phys. Chem. Lett.*, **3**, 2517 (2012).
31. C. Du, X. Yang, M. T. Mayer, H. Hoyt, J. Xie, G. McMahon, G. Bischoping and D. Wang, *Angew. Chem. Int. Ed.*, **52**, 12692 (2013).
32. A. Paracchino, J. C. Brauer, J.-E. Moser, E. Thimsen and M. Graetzel, *J. Phys. Chem. C*, **116**, 7341 (2012).
33. K. Gelderman, L. Lee and S. Donne, *J. Chem. Educ.*, **84**, 685 (2007).
34. A. Goltzene, C. Schwab and H. Wolf, *Solid State Commun.*, **18**, 1565 (1976).
35. T. Jiang, T. Xie, W. Yang, L. Chen, H. Fan and D. Wang, *J. Phys. Chem. C*, **117**, 4619 (2013).
36. S. Shyamal, P. Hajra, H. Mandal, A. Bera, D. Sariket, A. K. Satpati, S. Kundu and C. Bhattacharya, *J. Mater. Chem. A*, **4**, 9244 (2016).
37. A. Musa, T. Akomolafe and M. Carter, *Sol. Energy Mater. Sol. Cells*, **51**, 305 (1998).
38. M. Futsuhara, K. Yoshioka and O. Takai, *Thin Solid Films*, **317**, 322 (1998).
39. J. Hernandez, P. Wrschka and G. Oehrlein, *J. Electrochem. Soc.*, **148**, G389 (2001).
40. W. W. Gärtner, *Phys. Rev.*, **116**, 84 (1959).
41. Y. Liu, H. K. Turley, J. R. Tumbleston, E. T. Samulski and R. Lopez, *Appl. Phys. Lett.*, **98**, 162105 (2011).
42. K. Khan, Y. Leung and J. Kos, *Renew. Energy*, **11**, 293 (1997).

Supporting Information

Expanding depletion region via doping: Zn-doped Cu_2O buffer layer in Cu_2O photocathodes for photoelectrochemical water splitting

Kangha Lee[*], Cheol-Ho Lee[*,*], Jun Young Cheong[**], Seokwon Lee[*], Il-Doo Kim[**], Han-Ik Joh[***,****], and Doh Chang Lee[*,†]**

*Department of Chemical and Biomolecular Engineering (BK21+ Program), KAIST Institute for the Nanocentury, Korea Advanced Institute of Science and Technology (KAIST), Daejeon 34141, Korea
**Department of Materials Science and Engineering, Korea Advanced Institute of Science and Technology (KAIST), Daejeon 34141, Korea
***Carbon Convergence Materials Research Center, Institute of Advanced Composite Materials, Korea Institute of Science and Technology (KIST), Wanju, Jeollabukdo 55324, Korea
****Department of Extreme Energy Engineering, Konkuk University, Seoul 27478, Korea
(*Received 4 July 2017 • accepted 9 August 2017*)

XPS analysis was performed to see the valence state of incorporated Zn atoms in Cu_2O. The Zn 2p3 peak position in Zn : Cu_2O layer is located around 1,020 eV, whereas the Zn 2p3 peak position of ZnO has been reported to be centered at 1,022.4 eV [1,2]. The shift of XPS peak position indicates that doped zinc does not exist as pore ZnO but is more likely present a Zn^{2+} Zn-O-Cu brides [3,4].

Fig. S3 shows the result of the measurement for photocurrent generation by Zn : Cu_2O on FTO. The thickness of Zn : Cu_2O is the same as that of Zn : Cu_2O buffer layer on Cu_2O. Thin Zn : Cu_2O layer generates lower photocurrent by two to three orders of magnitude than bare Cu_2O layer. In addition, Zn : Cu_2O shows the only anodic photo-response. Therefore, we can assume that charge generation by Zn : Cu_2O has no effect on the significant increase of cathodic photocurrent generation over the positive potential range (0.6-1 V vs. RHE) and Zn : Cu_2O buffer layer has a synergetic effect only on charge separation.

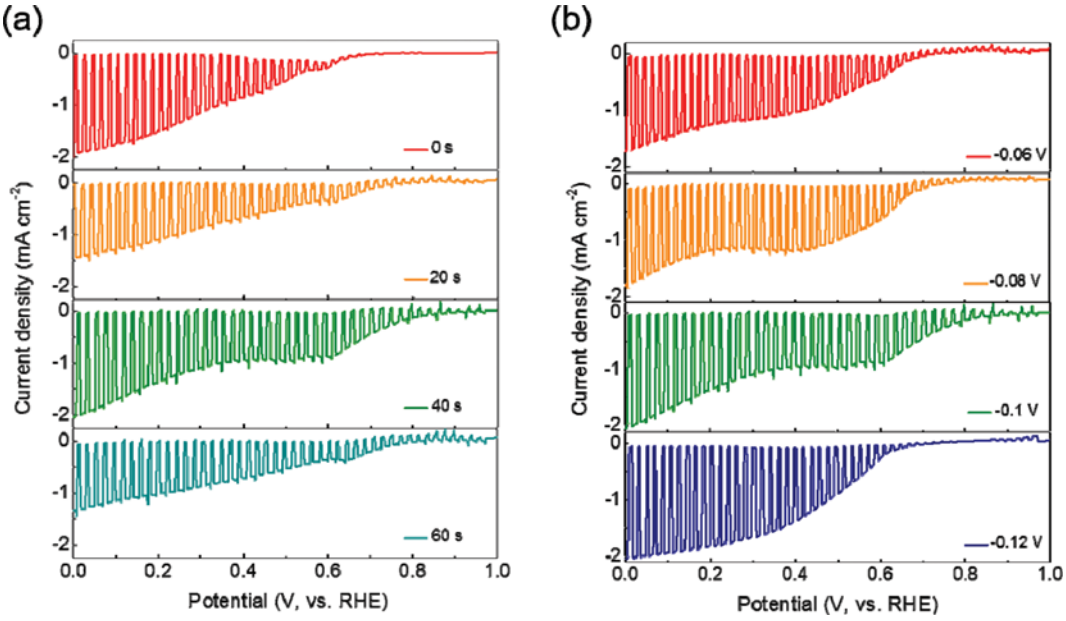

Fig. S1. (a) Light-chopped linear sweep voltammograms (LSV) for Cu_2O and Zn : Cu_2O/Cu_2O photocathodes depending on the electrodeposition time of Zn : Cu_2O buffer layer. The longer deposition time presents the thicker Zn : Cu_2O layer. (b) Light-chopped LSV for Zn : Cu_2O/Cu_2O photocathodes depending on the applied potential of Zn : Cu_2O buffer layer. More zinc atom is incorporated into Cu_2O when applied potential is more negative.

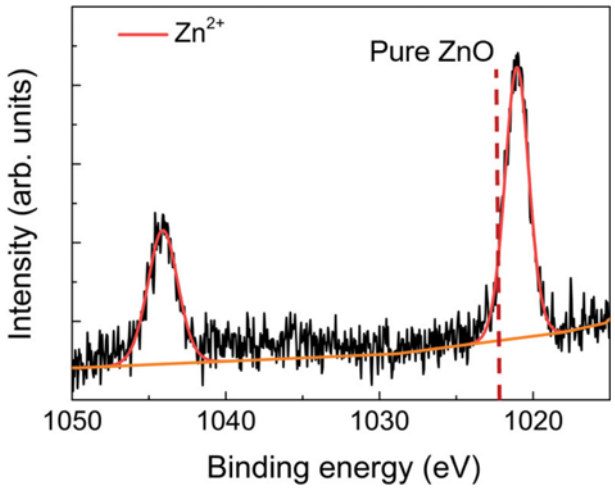

Fig. S2. X-ray photoelectron spectroscopy (XPS) spectrum of Zn 2p3 of Cu_2O/Zn : Cu_2O (dash line: binding energy of pure ZnO).

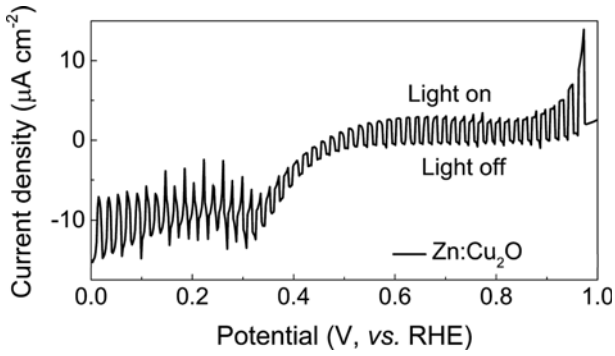

Fig. S3. Light-chopped LSV for Zn : Cu_2O electrochemically deposited on FTO glass for 40 s at 0.1 V vs. RHE.

REFERENCES

1. M. Chen, Z. Pei, C. Sun, L. Wen and X. Wang, *J. Cryst. Growth*, **220**, 254 (2000).
2. L. G. Mar, P. Y. Timbrell and R. N. Lamb, *Thin Solid Films*, **223**, 341 (1993).
3. B.-C. Lin, S.-Y. Chen and P. Shen, *Nanoscale Res. Lett.*, **7**, 1 (2012).
4. C. Zhu and M. J. Panzer, *ACS Appl. Mater. Interfaces*, **7**, 5624 (2015).